第35卷 第3期 焊 接 学 报 Vol. 35 No. 3
2014年3月 TRANSACTIONS OF THE CHINA WELDING INSTITUTION March 2014

不同应变速率下BGA焊球剪切断裂试验与模拟分析

薛明阳， 卫国强， 金 亮， 王海燕
(华南理工大学 机械与汽车工程学院，广州 510640)

摘 要：研究了BGA封装Sn-3.0Ag-0.5Cu无铅焊球经115 ℃时效后，焊球/铜界面IMC的形貌和组织变化，同时对BGA焊球在两种不同应变速率条件下的抗剪强度进行了分析，并运用ANSYS12.0软件对其过程进行2-D非线性有限元模拟. 试验结果表明，随着时效时间的延长，界面形貌由时效前的树枝状变成连续平坦的层状、界面IMC不断增厚，且焊球的抗剪强度随着时效时间的增加而不断降低；应变速率越高，抗剪强度越高. 模拟结果表明，应变速率越高，焊球经受的抗剪强度越大，Von Mises应力越大，等效塑性应变越小，塑性应变能密度越大.

关键词：BGA封装；抗剪强度；应变速率；有限元模拟
中图分类号：TG454 **文献标识码**：A **文章编号**：0253-360X(2014)03-0045-04

0 序 言

随着人们环保意识的提高，电子产品无铅化已成为全球化的发展趋势. 与其它无铅钎料相比，Sn-3.0Ag-0.5Cu钎料由于具有良好的钎焊工艺性能及综合力学性能在电子封装行业中得到广泛应用[1,2]. 但随着便携式电子产品的不断普及，互连焊点将承受高应变速率损伤(如跌落损伤)，造成新的焊点失效方式. 目前电子器件工程联合会(JEDEC)的《BGA焊球的剪切力测试标准JESD22-B117 2006》是评价焊球与封装基板结合强度最普遍的测试方法，但目前大多文献[3,4]研究的应变速率都比较低(小于0.7 mm/s)，主要目的是检验焊球和基板的结合强度. 基于此，文中研究了在等温时效条件下，不同应变速率(特别是高应变速率时)对BGA焊球抗剪强度的影响，并通过ANSYS有限元模拟对BGA焊点在变形过程中，焊点内部的应变场和应力场进行了分析，以便更深入的理解高应变速率下互连焊点的损伤机制.

1 试验方法和有限元模型

1.1 试验方法

试验采用镀铜的涂有OSP有机保护膜的PCB作为基板，焊盘直径为0.635 mm，焊球材料Sn-3.0Ag-0.5Cu，231 ℃回流3次. 将焊好的试样按合适的尺寸切割，并放入老化箱内进行时效试验，温度为115 ℃，时间分别为100，400，700和1 000 h. BGA焊球剪切试验在剪切试验机(型号为DAGE4000HS)上进行，剪切高度(剪切头与PCB板表面的距离)为0.06 mm，剪切速度分别为0.5和10 mm/s，每种速率下平均做25个焊球，抗剪强度取其平均值. 采用扫描电镜(SEM)观察BGA焊点的界面形貌.

1.2 有限元模型的建立和材料参数的选择

在建立高应变率条件下的BGA焊球模型时，为简化问题的求解，所建模型只包含焊球、铜焊盘、PCB基板以及剪切触头等主要部分. 且所有部分均采用2-D 8节点平面单元PLANE183模拟，有限元模型中共包含1 199个单元，3 617个节点. 图1a，b分别为剪切试验的焊球横断面实物图和有限元模型，其中焊球直径为0.76 mm，高度为0.64 mm，铜焊盘直径为0.635 mm，厚度为0.05 mm，撞锤高度为0.06 mm，PCB基板的厚度为0.5 mm.

BGA焊球在剪切过程中会涉及到接触问题，因此模拟分析时，需要建立“接触对”，即把一个边界作为“目标面”，另外一个作为“接触面”. 考虑到剪切撞锤的刚度要比无铅焊球大很多，故需要在剪切锤和焊球之间建立一个面与面的刚—柔接触对，分别用目标单元Targe169和接触单元Conta172来模拟剪切锤和焊球之间的接触行为. 另外由于接触问题是一种高度非线性行为，增加了求解时收敛的难度，为保证计算完全收敛，采用增强的拉格朗日法(augmented lagrange method)进行迭代.

在模型中，假设焊球为弹塑性材料，其余的器件材料均为线弹性. 由于焊球的材料为多晶体，故其塑性基于Mises屈服准则的等强度硬化模型描述，

收稿日期：2012-12-14
基金项目：国家自然科学基金资助项目(广东省联合基金资助项目U0734006)；国家自然科学基金资助项目(51371083)

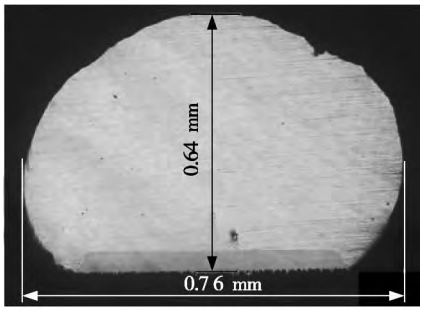

(a) 焊点回流后断面实物图

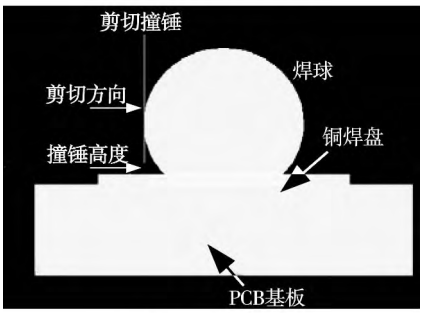

(b) 2–D有限元模型

图 1 剪切试验模型

Fig. 1 Solder ball shear test model

其材料属性见表 1[5] 和表 2[6]. 在剪切焊球试验中，PCB 板被完全固定，故求解前，假定焊球面为自由表面，PCB 板的右侧和底部施加全部约束，剪切触头施加竖直方向约束. 为方便与剪切试验结果进行对比，分别对剪切触头边缘加载水平方向速度 0.5 和 10 mm/s，剪切位移为 0.3 mm.

表 1 BGA 焊点封装器件的线弹性材料属性

Table 1 Linear elastic material properties for BGA assemblies

材料	杨氏模量 E/GPa	泊松比 μ	密度 ρ/(kg·m^{-3})
铜焊盘	127.7	0.34	8 900
PCB 基板	14.0	0.39	1 200
Sn-3.0Ag-0.5Cu 焊球	41.6	0.35	7 400

表 2 Sn-3.0Ag-0.5Cu 非线性各向同性硬化参数

Table 2 Multilinear isotropic hardening materials parameters for Sn-3.0Ag-0.5Cu

应力 σ/MPa	塑性应变 ε
20.8	0.000 5
46.0	0.021 1
48.0	0.041 1

2 结果与讨论

2.1 时效对焊点界面的影响

图 2a，b，c 分别为 Sn-3.0Ag-0.5Cu 钎料与铜焊盘在不同时效时间下 IMC(界面化合物) 的微观形貌. 由图 2a 可知，回流 3 次后，钎料与铜焊盘反应，界面 IMC 呈树枝状向钎料一侧延伸，经 EDX 分析，为 Cu_6Sn_5 相. 当时效时间为 400 h 时，界面 IMC 的厚度明显增加，并且界面形貌由凹凸不平的树枝状变成连续平坦的层状，钎料内部的 Ag_3Sn 晶粒明显粗化(图 2b). 当时效时间增至 1 000 h(图 2c)，在焊点内部出现了 Cu_6Sn_5 相，且界面 IMC 继续增厚，出现两层但没有明显的分界面，经 EDX 分析，较厚的呈灰色的上层为 Cu_6Sn_5，较薄的下层为 Cu_3Sn. 这是由于在时效过程中，先形成的 Cu_6Sn_5 相减缓了界面层的铜向钎料一侧扩散，因此 Cu 元素只能与 Cu_6Sn_5 反应形成了 Cu_3Sn[7].

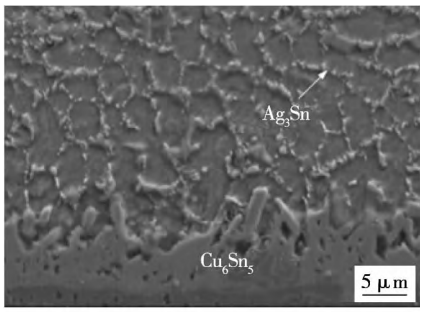

(a) 回流3次 (时效时间0 h)

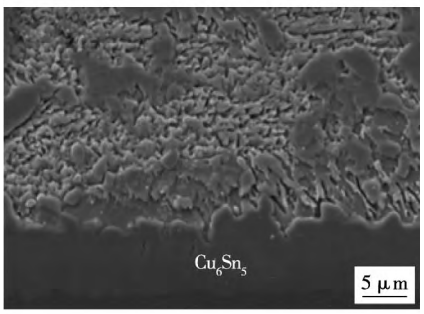

(b) 时效时间400 h

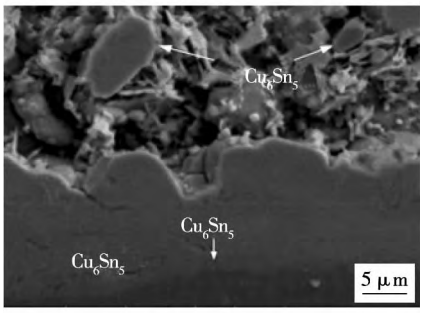

(c) 时效时间1 000 h

图 2 不同的时效时间下的界面 IMC 形貌(115 ℃)

Fig. 2 Morphology of interfacial IMCs for different aging time at 115 ℃

2.2 时效和应变速率对焊球剪切性能的影响

由图 3 可知，在 0.5 和 10 mm/s 两种剪切速率

下，未时效的 BGA 焊球抗剪强度最大，分别为 35.4 和 48.9 MPa. 随着时效时间的延长，Sn-3.0Ag-0.5Cu焊点的抗剪强度逐渐降低，当时效时间增至 1 000 h 时，两种速率下的抗剪强度分别降至 18.3 和 28.5 MPa，与未时效时相比，分别下降了 48.3% 和 41.7%. 此外在相同的时效条件下，剪切速率为 10 mm/s的焊球抗剪强度均高于 0.5 mm/s 时的抗剪强度.

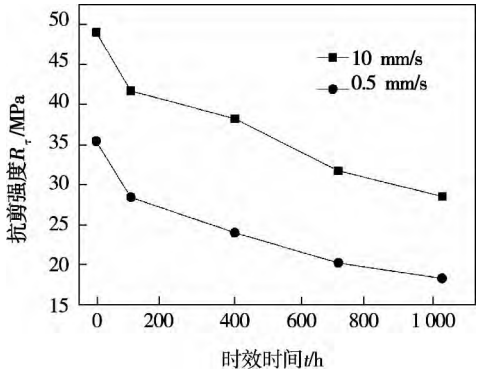

图 3　不同条件下 Sn-3.0Ag-0.5Cu 焊球抗剪强度变化

Fig. 3　Shear strength for Sn-3.0Ag-0.5Cu solder joint under different conditions

图 4a，b 分别为两种剪切速率下 Sn-3.0Ag-0.5Cu 焊球的 Von Mises 应力分布. 从两图中可知，Von Mises 最大应力均位于 BGA 焊球与铜焊盘接触的偏右位置，且当剪切速率较大时，焊球所表现出来的等效应力也相应地较大. 这是由于在塑性变形中，当应变速率较大时，除了施加给焊球的能量较多外，主要是由于位错移动速度远低于材料变形速率时引起的应变硬化致使塑性变形持续进行所需的应力增加.

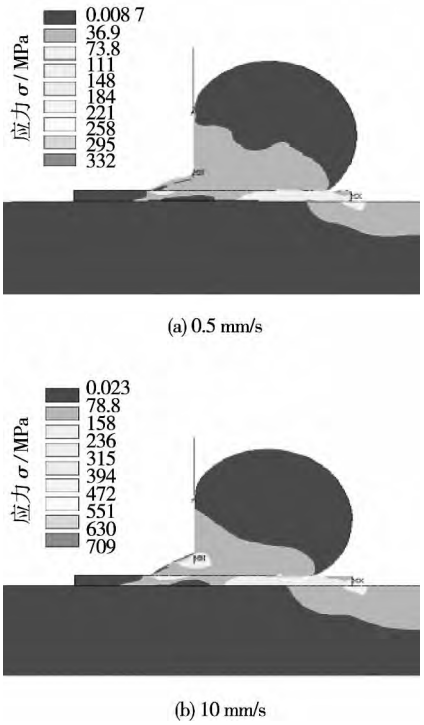

图 4　不同剪切速率下 Sn-3.0Ag-0.5Cu 焊球 Von Mises 应力

Fig. 4　Von Mises stress distribution for Sn-3.0Ag-0.5Cu solder joint under various shear rates

在剪切推球过程中，焊盘上的焊球(尤其是焊球角落位置)所受的应力是非常复杂的，包括拉应力、剪应力和压应力，所以等效塑性应变决定着焊球的断裂模式[8]. 图 5a，b 分别为不同剪切速率下的等效塑性应变分布. 对比两图可知，到达相同的位置，焊球在 0.5 mm/s 剪切速率下的应变要比 10 mm/s 大，最大值分别为 2.912 和 2.02. 由此可知，Sn-3.0Ag-0.5Cu 焊球的塑性等效应变随着应变速率的增大而减小，且其沿着剪切方向也逐渐降低，焊球中部并未发现形变.

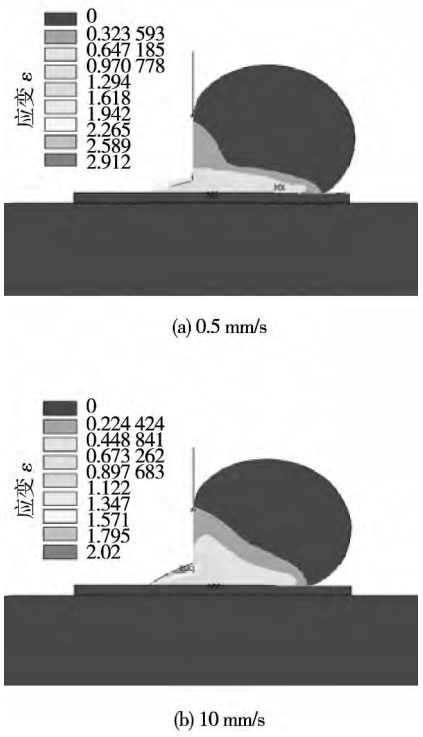

图 5　不同剪切速率下 Sn-3.0Ag-0.5Cu 焊球应变

Fig. 5　Von Mises strain distribution for Sn-3.0Ag-0.5Cu solder joint under various shear rates

由应变能密度理论可知，单位体积的应变能称为应变能密度，其值等于应力与应变之函数曲线所围的面积. 即

$$\omega = \int_0^{\varepsilon_{ij}} \sigma_{ij} \mathrm{d}\varepsilon_{ij}$$

式中：ω 为应变能密度；σ 为应力；ε 为应变.

假定焊球是由很多微小的单元组成的连续体，那么无论单元承受的是拉、压还是剪应力，应变能密度都能反映单元之间各应力分量的作用，因此塑性应变能密度可以对材料的塑性失效进行有效地预测[9,10]. 从图 6a，b 可知，在剪切速率为 0.5 mm/s 时，塑性应变能密度最高点分别在靠近于焊球与剪切触头处以及焊球与铜焊盘的接触位置，当增至 10 mm/s 时，其最高点则仅位于剪切触头与焊球的接触位置. 此外随着应变速率的增大，塑性应变能密度也呈增大趋势. 这意味着塑性应变能密度高的位置很容易造成裂纹的萌生和生长，最终使焊球失效.

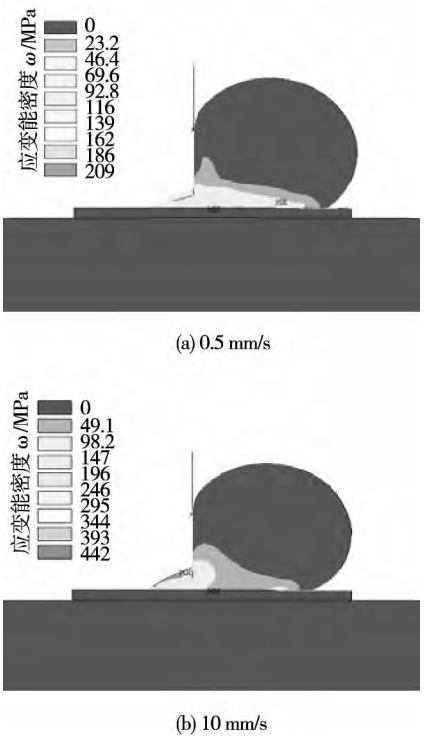

图 6 不同剪切速率下 Sn-3.0Ag-0.5Cu 焊球塑性应变能密度

Fig. 6 Plastic strain energy density distribution for Sn-3.0 Ag-0.5Cu solder joint under various shear rates

3 结 论

(1) 随着时效时间的延长，Sn-3.0Ag-0.5Cu/Cu 界面 IMC 的厚度不断增加，界面形貌由时效前的树枝状变为连续平坦的层状，界面成分由单一的 Cu_6Sn_5 逐渐转变为 Cu_6Sn_5 和 Cu_3Sn 两相，BGA 焊球的抗剪强度呈持续下降趋势.

(2) 应变速率对焊球的应力、塑性应变及应变能密度都有影响. 应变速率越高时，BGA 焊球抗剪强度越高，所受的 Von Mises 应力越大，等效塑性应变越小，塑性应变能密度越大，很容易造成裂纹的萌生和生长，导致焊球的失效.

参考文献:

[1] 刘 平，顾小龙，赵新兵，等. 不同 Ag 元素含量 Sn-Ag-Cu 无铅钎料性能分析[J]. 焊接学报，2012，33(6)：55－58.
Liu Ping，Gu Xiaolong，Zhao Xinbing，*et al*. Properties of Sn-Ag-Cu lead free solders with different silver content [J]. Transactions of the China Welding Institution，2012，33(6)：55－58.

[2] 万忠华，卫国强，师 磊，等. 低银 SnAgCuBiNi 无铅钎料润湿及溶解行为研究[J]. 焊接学报，2011，32(10)：89－92.
Wan Zhonghua，Wei Guoqiang，Shi Lei，*et al*. Analysis on wettability and dissolution behavior of low Ag SnAgCuBiNi lead-free solder alloys [J]. Transactions of the China Welding Institution，2011，32(10)：89－92.

[3] Kim J W，Kim D G，Jung S B. Mechanical strength test method for solder ball joint in the BGA package [J]. Metals and Materials International，2005，11(2)：121－129.

[4] Kim J W，Jung S B. Reexamination of the solder ball shear test for evaluation of the mechanical joint strength [J]. International Journal of Solids and Structure，2006，43(7/8)：1928－1945.

[5] Alam M O，Lu H，Bailcy C. Shear strength analysis of ball grid array (BGA) solder interfaces [C] // 9th Electronic Packaging Technology Conference，2007：770－773.

[6] Tseng S C，Chen R S，Lio C C. Sress analysis of lead-free solder with under bump metallurgy in a wafer level chip scale package [J]. The International Journal of Advanced Manufacturing Technology，2006，31(1/2)：1－9.

[7] 秦 飞，安 彤，仲伟旭，等. 无铅焊点金属间化合物的纳米压痕力学性能[J]. 焊接学报，2013，34(1)：25－28.
Qin Fei，An Tong，Zhong Weixu，*et al*. Nanoindatation properties of intermetallic compounds in lead-free solder joints [J]. Transactions of the China Welding Institution，2013，34(1)：25－28.

[8] Kim J W，Jung S B. Optimization of shear test for flip chip solder bump using 3-dimensional computer simulation [J]. Microelectronic Engineering，2005，82(3/4)：554－560.

[9] 孙 倩，李树忱，冯现大，等. 基于应变能密度理论的岩石破裂数值方法研究[J]. 岩石力学，2011，32(5)：1575－1582.
Sun Qian，Li Shuchen，Feng Xianda，*et al*. Study of numerical simulation method of rock fracture based on strain energy density theory [J]. Rock and Soil Mechanics，2011，32(5)：1575－1582.

[10] Li Q M. Strain energy density failure criterion [J]. International Journal of Solid and Structure，2001，38(38/39)：6997－7013.

作者简介：薛明阳，女，1986 年出生，硕士研究生. 主要从事无铅电子封装研究. 发表论文 1 篇. Email：mingyangxue112@126.com

通讯作者：卫国强，男，副教授. Email：gqwei@scut.edu.en

Abstract: A coupled thermal-mechanical FE (finite element) model of 7A52 aluminum alloy TANDEM welding and a simplified FE model for single-GCr15 shot impact simulation were developed separately. The element size of welded joint region which was impacted by shots was amplified reasonably. Based on the premise, the numerical results would not be affected by this simplification. The computational results of welding residual stress were obtained, and the influences of ball's dimension and impact velocity on induced residual stresses were analyzed subsequently. On the basis, the coupling computation of residual stress field in aluminum alloy welded joint and the shot peening treatment were performed by means of data transfer based on the standard and explicit solver of ABAQUS software. The computational results showed that the residual stresses on the surface and depth direction of welded joint were improved remarkably after shot peening.

Key words: aluminum alloy; welded joint; shot peening; finite element method; residual stress

Study on vacuum brazing of DD3 Ni-base superalloy and Ti_3AlC_2 ceramic LIU Jiakun[1], QI Junlei[1], CAO Jian[1], LIN Xingtao[2], WANG Zhijie[1], FENG Jicai[3] (1. State Key Laboratory of Advanced Welding and Joining, Harbin Institute of Technology, Harbin 150001, China; 2. Zhejiang Provincial Special Equipment Inspection and Research Institure, Hangzhou 310020, China; 3. Shandong Provincial Key Laboratory of Special Welding Technology, Harbin Institute of Technology at Weihai, Weihai 264209, China). pp 41 - 44

Abstract: By comparison, an appropriate brazing filler metal was selected and applied to the follow-on experiments. DD3 Ni-base superalloy and Ti_3AlC_2 ceramic were successfully brazed in vacuum using Ag-Cu-Ti as filler metal in a temperature range of 800 ~ 900 ℃ for 10 min. The interfacial microstructure of the brazed joints was investigated by adopting scanning electron microscope, energy dispersive spectroscopy and X-ray diffraction. The result showed that the typical interfacial microstructure of the joints can be described as DD3/AlNi/Al_3(Ni, Cu)$_5$ + Al(Ni, Cu) + Ag_{ss}/(Al, Ti)$_3$(Ni, Cu)$_5$/Al_4Cu_9 + $AlNi_2Ti$ + Ag_{ss}/TiAg/Ti_3AlC_2. Through the mechanical properties test of the joints, a maximum shear strength value of 135.9 MPa was obtained when the joint was brazed at 850 ℃ for 10 min. The fracture occurred at the Ti_3AlC_2 ceramic side adjacent to the brazed seam during the shear test. The interfacial microstructure of the joints was similar to each other, while the shear strength decreased when reduces or improves the brazing temperature.

Key words: superalloy; ceramic; brazing; interfacial microstructure; shear strength

Experimental and simulation analysis on shear fracture for BGA solder ball under different strain rates XUE Mingyang, WEI Guoqiang, JIN Liang, WANG Haiyan (School of Mechanical and Automotive Engineering, South China University of Technology, Guangzhou 510640, China). pp 45 - 48

Abstract: Influence of thermal aging time on the morphology and microstructure of the interfacial IMC for BGA (ball grid array) package between Sn-3.0Ag-0.5Cu lead-free solder ball and Cu interface at 115 ℃ were investigated. Meanwhile, the shear strength for BGA solder ball was studied and simulated by ANSYS 12.0 finite element software with a non-linear finite element model under two different strain rates. The experimental results are as follows: with the increase of the aging time, the morphology of interfacial IMC changes from dendritic to continuous even lamellar, the thickness of interfacial IMC increases continuously and the shear strength of solder ball gradually decreases. Furthermore, the simulation results show that the larger strain rate will result in the higher shear strength, the higher Von Mises stress, the smaller plastic strain and the higher plastic strain energy density.

Key words: BGA package; shear strength; strain rate; finite element analysis

Acoustic field modeling of ultrasonic-arc hybrid welding system and analysis of ultrasonic-aided arc pressure WANG Bin[1], SUN Qingjie[1,2], CHENG Wenqian[1], FENG Jicai[1] (1. Shandong Provincial Laboratory of Special Welding Technology, Harbin Institute of Technology at Weihai, Weihai 264209, China; 2. State Key Laboratory of Advanced Welding and Joining, Harbin Institute of Technology, Harbin 150001, China). pp 49 - 52

Abstract: Acoustic field analysis of space wave propagation used for ultrasonic-aided TIG welding was proposed and finite element simulation analysis of sound field variation with acoustic emission radius and that of the acoustics parameters variation with arc length was employed with COMSOL. Besides, a new model was also established for ultrasound-aided TIG welding characteristics. Distribution of arc pressure for stable combustion DC U-TIG arc and that of conventional TIG arc under different welding parameters were measured experimentally by using a hole drilling method. The result reveals that arc peak pressure of DC U-TIG is significantly higher than that of conventional TIG, which illustrates that the effect of hybrid-arc can enhance the arc pressure above the surface of weld pool, but the D-value between them decreases with the welding current increases. Preliminary analysis suggests that when high welding current is employed, the high temperature and large current density in the central area of arc column greatly improve the arc peak pressure of conventional TIG. In contrast, the increase of arc peak pressure is reduced with the increase of weld current because plasma flow force of welding arc is limited by gas-flow rates.

Key words: ultrasonic hybrid; acoustic field modeling; arc pressure

Active brazing of SiO_{2f}/SiO_2 composite and Invar alloy with Cu-25Sn-10Ti ZHANG Dalei[1], QI Junlei[1], ZHANG Lixia[1], FENG Jicai[2], LIANG Yingchun[3] (1. State Key Laboratory of Advanced Welding and Joining, Harbin Institute of Technology, Harbin 150001, China; 2. Shandong Provincial Key Laboratory of Special Welding Technology, Harbin Institute of Technology at Weihai, Weihai 264209, China; 3. School of Mechatronics Engineering, Harbin Institute of Technology, Harbin 150001, China). pp 53 - 56

Abstract: The Invar alloy was brazed to SiO_{2f}/SiO_2 com-